International Journal of Heat and Mass Transfer 180 (2021) 121744

Contents lists available at ScienceDirect

International Journal of Heat and Mass Transfer

journal homepage: www.elsevier.com/locate/hmt

Machine learning predictions of critical heat fluxes for pillar-modified surfaces

Brandon Swartz [a], Lang Wu [b], Qiang Zhou [b,*], Qing Hao [a,*]

[a] Dept of Aerospace and Mechanical Engineering, University of Arizona, Tucson, AZ 87521, USA
[b] Dept of Systems and Industrial Engineering, University of Arizona, Tucson, AZ 85721, USA

ARTICLE INFO

Article history:
Received 1 March 2021
Revised 10 June 2021
Accepted 12 July 2021
Available online 25 July 2021

Keywords:
Machine learning
Critical heat flux
Mean beam length
Pool boiling
Random forest

ABSTRACT

For convection research, one important topic is the maximum heat flux achieved on a boiling surface, known as the critical heat flux (CHF). This phenomenon is characterized by the formation of a blanket of heat-blocking vapor on the surface. Over several decades, numerous surface structures have been fabricated to enhance the CHF for various high-power cooling applications. However, the complexity of the surface structures and many other factors (e.g., capillary wicking flux) restrict the prediction of the CHF using theoretical models. In this work, three popular machine learning (ML) methods are employed to analyze and further predict the CHFs for a given surface modified with micro-structures. Among these, the random forest regression method consistently produced the best fitting models of previously published data. The importance analysis algorithm developed for random forest models facilitated efficient discovery of the most important descriptors predicting the CHF. One key descriptor used in these models was the mean beam length (MBL), a terminology borrowed from radiative heat transfer, which effectively described the characteristic spacing between adjacent surface features. The models showed greatest sensitivity to the MBL and the height of the features, compared to the other surface descriptors.

1. Introduction

Boiling is characterized by very large heat transfer coefficients and is therefore used in applications that require rapid heat removal. The maximum practical heat flux that can be achieved through boiling is limited by the CHF, which occurs when the vapor produced on the boiling surface coalesces into a vapor film, drastically impeding further heat transfer and leading to a rapid surface temperature increase.

In the literature, a few analytical models have been developed. A majority of models can be expressed in the non-dimensional form derived by Kutateladze [1] using dimensional analysis,

$$K = \frac{q''_{CHF}}{h_{fg}\left[\sigma g \rho_g^2 (\rho_l - \rho_g)\right]^{\frac{1}{4}}} \tag{1}$$

Models with this form have since been derived based on proposed triggering mechanisms of bubble interference, hydrodynamic instability, macrolayer dryout, irreversible dry spot growth, and macrolayer "lift-off" [2]. Although there has been disagreement in the triggering mechanism, these models consistently have the same general form, indicating agreement in the major impacts of fluid properties on the CHF. However, these models do not account for the impact of surface morphology.

The impact of surface morphology and material on the CHF has been proposed to be due to surface area enhancement, wettability, capillary wicking, nucleation site density, and separation of liquid and vapor flow paths [3]. Due to the complexity of these phenomena, previous models are either limited in scope or require further measurements on parameters such as capillary wicking flux [4] or dynamic liquid contact angle [5]. These impair the model's usefulness in predicting an optimized CHF, particularly for the optimization of surface structures in pursuit of an even higher CHF.

By analyzing the forces acting on a surface bubble, Kandlikar [5] developed another popular model for the CHF incorporating the impact of contact angle and surface orientation relative to horizontal:

$$K = \frac{1+\cos\theta}{16}\left[\frac{2}{\pi} + \frac{\pi}{4}(1+\cos\theta)\cos\psi\right]^{\frac{1}{2}}, \tag{2}$$

where K is defined in Eq. (1). Kandlikar proposed to use the dynamic receding contact angle; however it has been common to use the static contact angle at room temperature, which is easier to measure and usually only makes a small difference in the model

* Corresponding authors.
E-mail addresses: zhouq@email.arizona.edu (Q. Zhou), qinghao@email.arizona.edu (Q. Hao).

https://doi.org/10.1016/j.ijheatmasstransfer.2021.121744
0017-9310/

Nomenclature

CHF	critical heat flux
DFNN	deep feedforward neural network
DT	decision tree
MBL	mean beam length
ML	machine learning

Greek symbols

ρ_g	vapor density
ρ_l	liquid density
θ	contact Angle
σ	surface tension
ϕ	porosity
ψ	surface orientation angle

Roman symbols

g	gravitational acceleration
h	surface feature height
h_{fg}	latent heat of vaporization
K	dimensionless critical heat flux
q''_{CHF}	critical heat flux
r	roughness factor

prediction [6]. Kandlikar's model correctly predicts that superhydrophilic surfaces will have higher CHF values; however, at small contact angles, Kandlikar's model saturates to a constant value that generally underestimates the CHF of these surfaces [7].

Chu et al. [8] improved Kandlikar's model by expanding upon the impact of roughness, which was defined as the ratio of the true surface area in contact with the liquid to the apparent or "projected" area. The inherent limitation of Chu's model is that it is not sensitive to the specific geometry of the structures, which can also influence the capillary wicking and separation of liquid and vapor paths.

Several other authors have proposed models that account for the impact of capillary wicking using experimentally measured parameters such as the wicking coefficient, absorption rate, or wicked volume flux [4,6]. The reported accuracy of these models suggests capillary wicking is an important mechanism for the CHF enhancement. However, these models require fabricating and testing each surface before a prediction can be made, which limits their practical use. Li and Huang [6] developed a model to account for capillary wicking based on surface material and morphology. This avoids the issue of requiring complex experimental measurements but at a cost of decreased model scope and accuracy. Nonetheless, by considering the specific shape of surface structures instead of solely using the surface roughness, Li's model was able to capture previously observed behaviors that were not accounted for by previous models.

Other than analytical models, machine learning has been previously used to model various aspects of flow boiling and pool boiling, though few groups have included the influence of surface morphology. Neural networks have been used to model flow boiling heat flux [9], CHF [10–13], heat transfer coefficient [14–16], maximum wall temperature [17], and onset of nucleate boiling [18]. Surface morphology has a reduced importance for flow boiling, so these previous studies have been able to accurately model flow boiling behaviors only based on the overall geometry and flow parameters.

For pool boiling, neural networks have been used to model minimum film boiling temperature during quenching of rods [19] and pool boiling with nanofluids [20–23]. Das and Kishor [24] used fuzzy systems to model heat transfer coefficients for pool boiling of water on plain tubes. Random forest regressions have also been applied to model the CHF in flow boiling [10]. These models have incorporated fluid properties, flow parameters, and overall geometry, but have not considered enhanced microscale surface morphologies.

As the only model to consider specific microscale surface morphologies, He and Lee [25] used neural networks to model the CHF on silicon pin fin surfaces. They observed that deep belief networks were most suitable for CHF modelling compared to other neural network types. Their models fit the data very well but were significantly limited in scope and did not present an obvious means of expanding their model to other surface types.

In this work, a new data-driven model has been developed using machine learning, which improves upon previous pool boiling models by directly accounting for surface morphology using fundamental surface descriptors. As a first step, data was collected for the reported CHFs from surfaces with pin-fin arrays, which allowed for rapid calculation and testing of proposed descriptors used as inputs for the machine learning model. All of the surface descriptors used in the models can be easily calculated based solely on geometric surface properties and are not necessarily limited to pin-fin array surfaces. Three popular machine learning methods (random forests, linear lasso, and neural network) were applied to make CHF predictions based on surface geometry descriptors and to investigate the sensitivity of the models to each descriptor. One key descriptor used in these models was the mean beam length (MBL), a term borrowed from radiative heat transfer, which effectively described the characteristic spacing between adjacent surface features. The models showed greatest sensitivity to the MBL and the height of the features, compared to the other surface descriptors. Root mean squared relative error (RMSRE), mean absolute relative error (MARE) and coefficient of determination (R^2) were used to measure the accuracy of machine learning models, which showed greatest accuracy for the random forest method (with R^2 up to 0.986). The success in using these descriptors suggests the possibility of expanding this model to a broader scope of surface morphologies and surface materials, eventually leading to a general model for the CHF that applies to all types of surface modifications.

2. Machine learning models

Three machine learning methods were applied: linear LASSO (Least Absolute Shrinkage and Selection Operator) [26], deep feedforward neural networks (DFNN) [27], and random forest [28].

Linear regression is the most common statistical method for predictive modeling. LASSO is a type of advanced linear regression that includes regularization factors to avoid overfitting and lower model complexity. Whereas the cost function in typical linear regression is the sum of squared errors, in LASSO regression, the cost function is modified by adding the L_1 norm of the coefficients, $\boldsymbol{\beta}$, as a penalty such that the cost function is penalized if the coefficients are large. The coefficients are calculated by minimizing this cost function, as shown in Eq. (3), where $\mathbf{X}$ represents the matrix of input descriptors, $\mathbf{y}$ is the actual CHF values, and the λ is the tuning parameter.

$$\hat{\boldsymbol{\beta}}_{lasso} = \underset{\beta}{\operatorname{argmin}} \ \|\boldsymbol{y} - \boldsymbol{X}^T\boldsymbol{\beta}\|_2^2 + \lambda\|\boldsymbol{\beta}\|_1 \tag{3}$$

The additional term in the cost function shrinks the coefficients and helps to overcome multicollinearity. This form of regularization might result in certain coefficients being absolutely zero, implying that some descriptors are totally ignored in the output evaluation. As a result, LASSO regression aids not only in the overfitting reduction but also the descriptor selection. However, there should be strong linear relationship between the inputs and response to make a good prediction with LASSO.

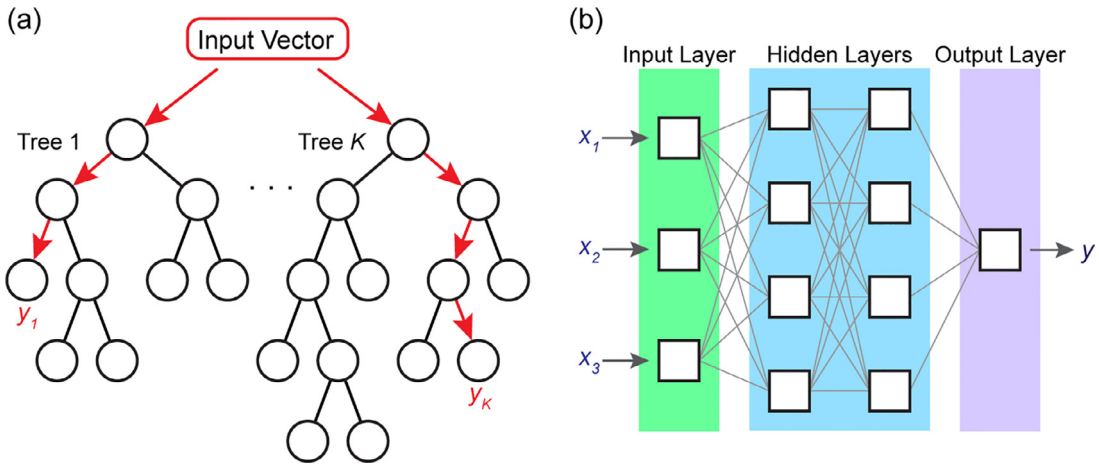

Fig. 1. Graphical representation of (a) random forest regressions and (b) artificial neural networks.

DFNN employs numerous layers of nodes, each of which is fully linked to the next layer (Fig. 1b). The surface descriptors and experiment parameters in our study are represented by a set of neurons in the input layer. Each hidden layer neuron is the result of a weighted sum of the neurons in the preceding layer, followed by an activation function that introduces non-linearity into the model. The output layer can comprise one or more nodes that gather the information processed from the last hidden layer, depending upon the problem type (classification or regression). Due to the emergence of backpropagation [29], which allows the network to alter the connection weights between layers when processing each batch of data, DFNN has grown in popularity over the last several decades. There are three commonly used activation functions in practice: sigmoid function, tanh function and rectified linear units (ReLU) [30]. However, sigmoid and tanh functions have the saturation problem (the gradient gets to near-zero) when dealing with deep neural networks. The 'Adam' solver proposed by Kingma et al. [31] is a stochastic gradient-based optimizer and usually a good choice in terms of both training time and validation score. Learning rate is a very important hyperparameter for training neural networks. Because a small learning rate may lead to a very slow convergence rate and potentially get trapped in a local optimum, whereas a large learning rate can make the training process unstable and even diverge. However, it is not necessary to manually adjust the learning rates with Adam optimizer because they will be adaptively selected for each parameter during the training process [32]. Based on some empirically-derived rules-of-thumb, the DFNN architecture applied here is X/50/50/50/1, with X the number of input descriptors. Generally speaking, the deeper the network, the more data required for training. We may not have a satisfactory result without enough data to train DFNN. Besides, the performance of DFNN is highly dependent on the hyperparameters applied in the training process, but there is no generic way to determine them.

Decision trees (DTs) [33] learn hierarchically by continuously dividing training samples into branches that maximize the information gain of each split. DTs work very well especially if they are of small depth. However, DTs with higher depth are more prone to overfitting and thus lead to higher variance in the model. This shortcoming of DT is overcome by the random forest model, which uses many uncorrelated DTs (Fig. 1a). The samples used to train each tree are randomly drawn with replacement, known as bootstrapping [34], which means that some samples may be used multiple times in a single tree. These bootstrap samples are then fed as training data to many DTs of large depths. Each of these DTs is trained separately on these bootstrap samples. This aggregation of DTs is called the random forest ensemble. For regression models, the final prediction is taken as the average of the prediction of each tree. The discrepancies in the original training dataset have no impact on the final result derived from the aggregate of DTs because each DT takes a different set of training data as input. The descriptor selected in each node is utilized to partition the data set into two different sets with similar responses (CHFs) inside. In the case of regression, we normally compare variance reduction to choose the descriptor, and the descriptor with the greatest decrease is chosen for that node. In addition, the descriptor importance can be measured based on how much the descriptor reduces the variance on average over all the trees in the forest. The ease of calculating relative descriptor importance makes the random forest method effective for informing descriptor selection. Our models use 50 trees to minimize overfitting; adding additional trees beyond this did not improve model performance. The best results were obtained with 50 leaf nodes per tree. Only 80% of the input descriptors are considered in each individual tree. Tuning parameters were optimized using 10-fold cross-validation. A limitation of random forest regressions is that they cannot be used for extrapolation [35]. The thresholds for the splits in each tree will always be within the domain of the training data inputs, therefore the trees cannot be used to predict how the performance will change outside of that domain.

3. Descriptors used for machine learning models

Boiling CHF data for a total of 175 surfaces from 16 representative papers [36] were collected and used to train and test ML models. The data include boiling of water on silicon surfaces and FC-72 on silicon or copper surfaces. Only flat surfaces and surfaces with periodic arrays of pin-fins were included in the data set, but otherwise the fin size, shape, and array pattern were not restricted. The data include circular, square, and octagonal fin shapes, and square and hexagonal unit cells for the array pattern. Some available papers were excluded from the dataset if their reported CHF for water on a smooth silicon surface was less than 700 kW/m^2 or greater than 850 kW/m^2, which limited the amount of variation due to differences in methods between previous experimental studies, thus allowing the data to better represent the impact of the surface morphology. Many combinations of descriptors for these surfaces were attempted in order to assess the relative importance and effectiveness of each descriptor for predicting the CHF. The tested surface descriptors include the fin width, spacing, height, total MBL, lateral MBL, roughness factor, porosity, and coverage. Descriptors for the fluid type and fluid subcooling were

also included in every ML model. The impact of environmental pressure was not included in these models; only data corresponding to boiling near one standard atmosphere was included in the dataset. Each of these descriptors was believed to be relevant to one or more previously proposed physical mechanisms for the CHF enhancement, such as wettability or capillary wicking. Identifying the fundamental surface parameters relevant to each CHF enhancement mechanism is progress towards a general model for the CHF.

Since almost all of the recent boiling experiments on pin fin surfaces have used either water or FC-72 as the test fluid, the dataset used in this study was not diverse enough to thoroughly evaluate the impact of fluid properties on the CHF. Both commonly tested fluids were incorporated into the model using a categorical descriptor.

Fluid subcooling describes the temperature difference between the bulk pool temperature and the saturation temperature of the fluid. Although subcooling is not a surface property, the subcooling descriptor was included in the models to allow the large amount of data on boiling with subcooling to be included in the models.

For heat conduction within a porous media, various descriptors have been introduced [37]. As a novel characteristic length, the MBL [38] is emphasized here for boiling:

$$MBL = \frac{4V_{fluid}}{A_{surface}}. \tag{4}$$

The term MBL is used because this length is similar to the geometric MBL used in radiation heat transfer, though in this context this length is unrelated to radiation. This characteristic length is proposed to be relevant to the capillary wicking and contact line pinning mechanisms. The volume used here was the fluid volume bounded by the projected area of the heated surface and the height of the surface features, i.e., $V_{fluid} = hA_{projected}\phi$, where h is the height and ϕ is the porosity. Two different surface area expressions were proposed and tested: the total surface area and the lateral surface area. When the lateral surface area is used, the MBL represents a characteristic spacing between the lateral surfaces of the fins. When the total surface area is used, the distance to the flat bottom surface is also considered. Using the same definition of the dimensionless roughness factor r used by Chu [8] and many others, the total and lateral surface areas can be expressed as $A_{total} = rA_{projected}$, and $A_{lateral} = (r-1)A_{projected}$. The total and lateral MBL can then be expressed in very general terms that could be applied to any boiling surface.

$$MBL_{total} = \frac{4h\phi}{r} \tag{5}$$

$$MBL_{lateral} = \frac{4h\phi}{r-1} \tag{6}$$

The coverage descriptor was used to partially account for the impact of heterogeneous surfaces. Coverage was defined as the fraction of the surface that was intentionally kept smooth. If the fin pattern was applied uniformly to the entirely surface, then the coverage value was unity. Only 25 data points in the set corresponded to boiling on heterogenous surfaces, and many of these data correspond to nominally identical surfaces tested at different subcooling temperatures, so there is not enough diversity in the data set to capture the impact of surface heterogeneity on the CHF. Future studies could expand upon this behavior if more heterogenous surfaces are included in the data set.

Although wettability – characterized by the contact angle – is known to be important to the boiling CHF [2], the contact angle was not included as a descriptor in our models. This was primarily because of limitations in the available data. Almost all of the collected data was either for copper or silicon surfaces. It was noted that reported CHFs for boiling of water on copper were generally higher though copper has lower wettability than silicon [4]. This behavior is in opposition with the currently accepted understanding of the impact of wettability on the CHF [2]. In order to accurately model the true impact of the contact angle on the CHF of micro-structured surfaces, a greater variety of surface materials is necessary.

Table 1
Accuracy of models using MBL descriptors. Model performance metrics are based on model prediction accuracy for a test data set that was not used in model training.

MARE	RMSRE	R^2	Length Descriptor	Other Descriptors
7.4%	9.2%	0.98	Width and Spacing	Subcooling, height,
7.8%	10.6%	0.91	Lateral MBL	coverage, fluid type
7.8%	10.4%	0.96	Total MBL	
6.6%	8.4%	0.986	Width and Spacing	Subcooling, height,
6.7%	8.5%	0.981	Lateral MBL	coverage, fluid type,
6.5%	8.5%	0.984	Total MBL	porosity, roughness

It was noted that papers studying the boiling of FC-72 had smaller relative variation in reported CHF values on smooth surfaces compared to the variation in the CHF for water. Due to its very low surface tension [39], FC-72 has a nearly zero contact angle on most surfaces, so the impact of different surface materials on the CHF is small. This allowed data for FC-72 on both silicon and copper surfaces to be included in the dataset, while data for water on copper surfaces was not included.

The domain of the input features is important for understanding limitations of the current models and the directions for future investigation. Fig. 2 shows the distribution of six of the descriptors considered in this study. The data for boiling of water only included microscale surfaces, while the both microscale and macroscale surfaces were included for boiling of FC-72. For most data in the dataset, the height, width, and spacing of the fins were all similar in magnitude, which limited the variation in the roughness factor and porosity of the surfaces. In order to move towards more general models for predicting the CHF, it is necessary to collect data from a wider variety of surfaces.

4. Results and discussion

Using random forest regressions, the MBL descriptor has proven to be effective for replacing the fin width and spacing descriptors, which is beneficial because the MBL is a more general characteristic length that could be applied to a wider scope of surfaces. The relative effectiveness of the total MBL as opposed to the lateral MBL was also evaluated. For these comparisons, only a small number of key surface descriptors were included, so as to better focus on the impact of the tested length descriptors. RMSRE, MARE and coefficient of determination (R^2) were used to measure the accuracy of the random forest model. For RMSRE and MARE, we first calculate the relative error for each test data by dividing the error (between estimated and true value) by the true CHF values and then compute the mean absolute value and root mean squared value of their relative errors.

There was a concern that the total MBL might be less effective because it is strongly dependent on the height of the structures and the height is already included as a separate descriptor. In contrast, for pin-fin surfaces, the lateral MBL is completely independent of height, and only depends on the size and spacing between fins. However, as seen in Table 1, the total MBL was found to be more effective for predicting the CHF than the lateral MBL. When the length descriptors are supplemented by only the subcooling, height, coverage, and fluid type descriptors, neither MBL descriptor quite matches the performance of using both the width and spacing descriptors. When roughness and porosity descriptors are added, the additional information allows the models to be reli-

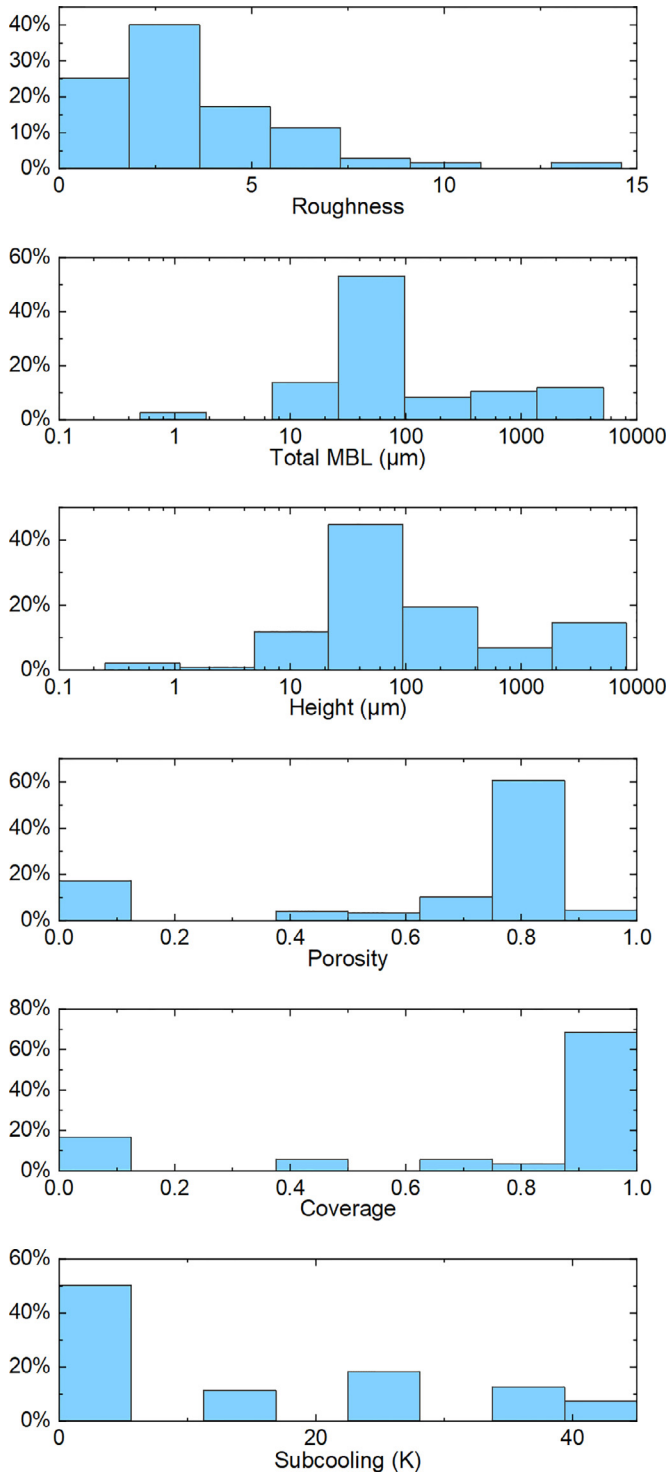

Fig. 2. Data distribution for six descriptors used in machine learning models.

ably accurate for any of the proposed length descriptors. Thus, the width and spacing descriptors can be replaced by the total MBL descriptor. Although the accuracy of the models is not significantly altered after switching to the MBL descriptor, the MBL is an improvement over the width and spacing descriptors because it is a more fundamental characteristic length. Whereas the width and spacing descriptors are only relevant to pin-fin surfaces, the MBL is meaningful for any type of surface enhancement. The discovery of more fundamental descriptors, such as the MBL, allows for the development of more general machine learning models for boiling critical heat flux.

Table 2
Relative importance analysis of tested descriptors.

Subcooling	Height	Coverage	Porosity	Total MBL	Roughness
0.229	0.403	0.019	0.017	0.218	0.114

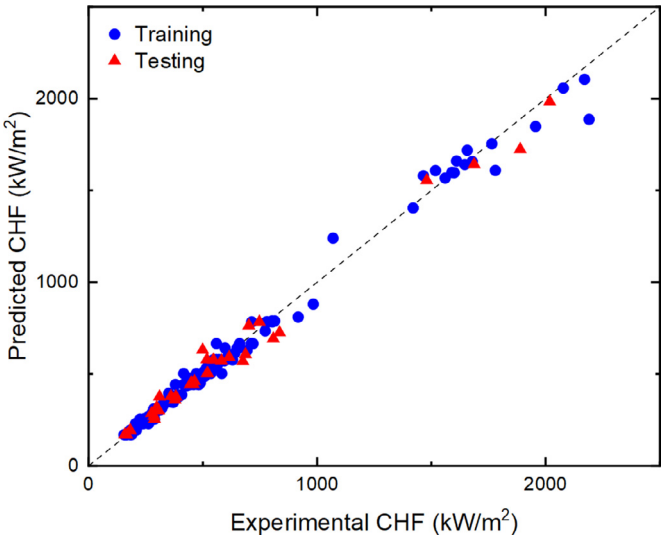

Fig. 3. Random forest regression using subcooling, roughness, height, total MBL, and fluid type descriptors.

The ability to easily perform importance analyses on descriptors used in a random forest regression model was found to be very helpful for identifying the most influential descriptors. Table 2 shows the results of an importance analysis performed on the best model from Table 1. It can be seen that the height, subcooling and total MBL demonstrate more significance than the other descriptors. The fluid type descriptor was not included in this analysis because its importance is obvious. The analysis shows that the porosity and coverage descriptors have a much smaller impact on the CHF compared to the other descriptors. It is interesting that the coverage descriptor has such a small impact. However, this is likely because there is not enough data for surfaces with non-unity coverage, so the model cannot yet accurately predict the impact of that feature. The result for porosity suggests that the porosity of pin fin surfaces does not have a large impact on the boiling performance.

A new model developed using only the subcooling, height, total MBL, roughness, and fluid type descriptors had almost identical model performance, shown in Fig. 3, compared to the previous model that also included coverage and porosity. This model is believed to be superior to the other models presented in this paper, because it maintains a similar accuracy to the highest performing models but requires less information.

Neural networks and linear LASSO algorithms were also attempted with various descriptor combinations throughout this study, but were not able to replicate the accuracy of the random forest regression algorithm for this dataset (see Table 3). This is attributed to the small size of the dataset and the large amount of uncertainty present in the CHF measurements. The random forest regression algorithm works well despite the limited amount of training data without overfitting to the random errors. Fig. 4 shows the RMSE time history for the neural network method. As the epoch increases, the training error decreases and the validation error becomes stable after 30 epochs. Fig. 5 illustrates the changes of the RMSRE versus the number of decision trees in the random

Table 3
Comparison of ML algorithms using descriptors of subcooling, height, total MBL, roughness, and fluid type.

Algorithm	MARE	RMSRE	R^2
Random Forest	6.2%	8.7%	0.98
Neural Network	20.7%	30.0%	0.91
Linear LASSO	19.0%	26.8%	0.84

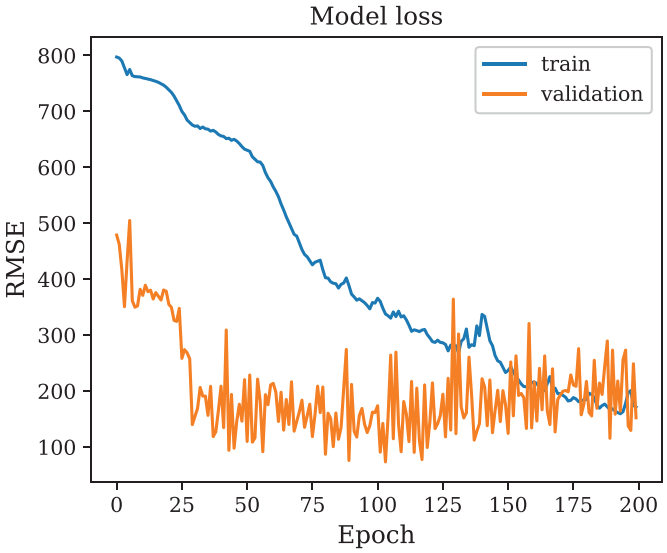

Fig. 4. RMSE time history for the neural network method. RMSE is the root mean squared error.

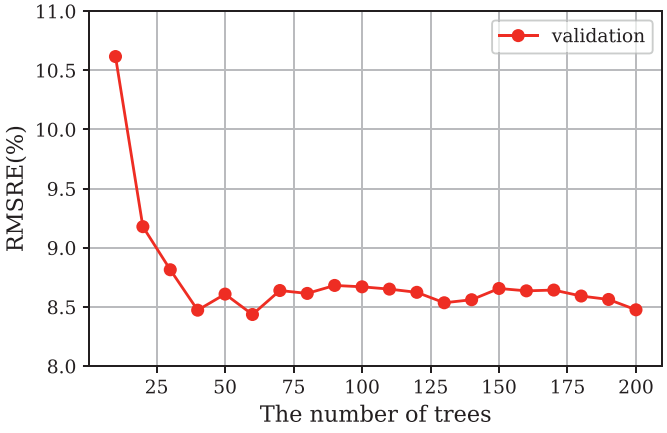

Fig. 5. RMSRE versus the number of decision trees in random forest

forest model. It can be observed that the RMSRE value decreases quickly as more trees are added but becomes stable after 50 decision trees. Therefore, 50 decision trees were used in the final random forest models to achieve a good prediction result.

In Fig. 6, our random forest model is compared to Chu's [8] and Li's [6] models. The ten compared points are drawn from the testing dataset. Data with subcooling was not included in the comparison because Chu and Li did not include the impact of subcooling in their models. This comparison shows that our random forest model has greater prediction accuracy for a wide range of pin fin surfaces. Necessary fluid properties for each model were drawn from published tables [39]. Intrinsic static contact angle data for each point was collected from the point's originating paper whenever possible. Many papers on FC-72 do not report the contact angle, so for FC-72 on silicon and SiO_2 surfaces, the intrinsic static

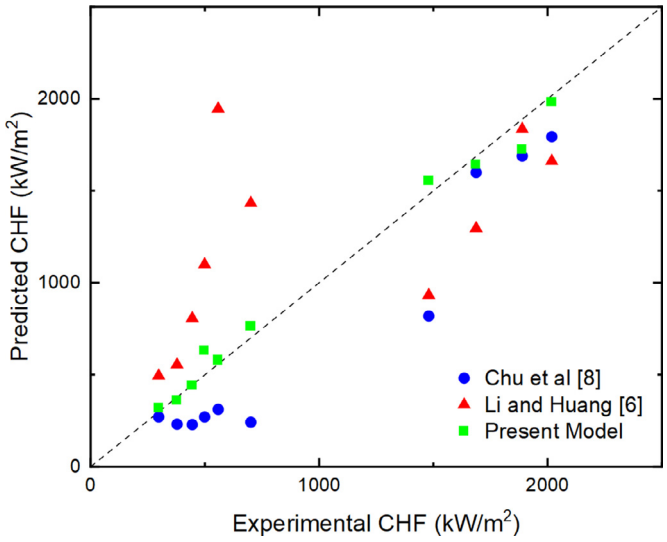

Fig. 6. Comparison of prediction accuracy with published CHF models for structured surfaces. To keep the comparison fair, only homogeneous surfaces tested without subcooling from the testing dataset are included.

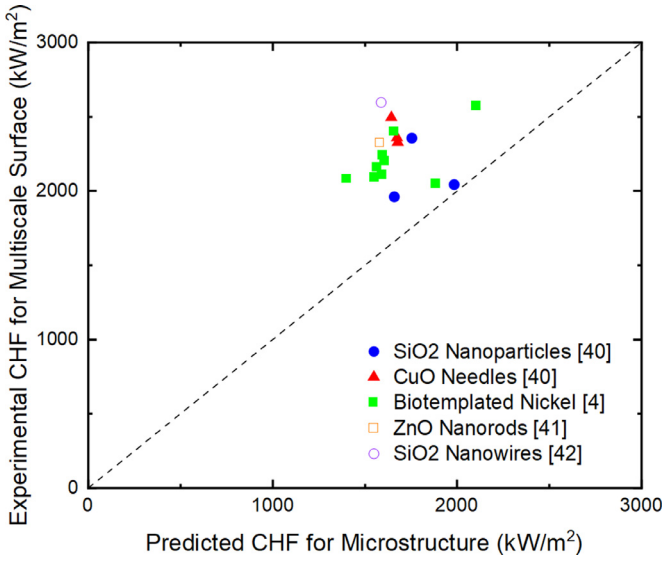

Fig. 7. Random forest regression model applied pin fins surfaces with an additional nanoscale surface enhancement.

contact angle was approximated as 1° for all surfaces [39]. This approximation has negligible impact on the referenced model predictions, which are only functions of the cosine of the contact angle and therefore are insensitive to small uncertainties in contact angle near zero degrees. When evaluating predictions for the models, all assumptions posed in Chu's and Li's papers were used, except for the correction suggested by Chu to account for change in contact angle between room temperature and saturation temperature. For FC-72, this correction would have little to no effect, because FC-72 already has a near zero contact angle. However, for water (the rightmost four points) this correction would result in a slight improvement to Chu's prediction accuracy.

Although our random forest model can only be directly applied to pin fin surfaces, it could also be useful for evaluating the relative enhancement of nanoscale features added to micro-pin-fin surfaces. Fig. 7 shows the results for five different nanoscale surface modifications for a micro pin fin surface [4,40–42]. All of the experimental CHF values for these surfaces are greater than the

predicted values, and the difference between the two can be attributed to the benefits from nanofeatures. Using the model in this way could allow for the interaction between nanoscale and microscale surface modifications to be studied.

The models developed in this study are limited to pin fin surfaces because they have only been trained using data for pin fin surfaces. However, the framework and systematic procedure for developing boiling CHF models could be extended to create models that apply for a greater scope of surface types. Data for additional surface types could be added to the training dataset and new fundamental descriptors could be added based on theoretical and optical studies of what surface morphological features are expected to impact boiling performance. Using random forest regressions, the importance of proposed descriptors can be quickly evaluated, which can streamline the process of descriptor selection. This procedure could be applied to generate accurate models with a large scope of applicability that thoroughly account for both known and unknown relationships between surface morphology and boiling performance.

5. Conclusion

The precise relationships between the boiling CHF and surface morphology are not well understood, which has limited the scope and accuracy of previous CHF models. However, the large body of boiling data that has been collected over the past several decades makes this relationship a good candidate for ML modelling. By using known physical behaviors to guide the selection of descriptors and verifying the effectiveness of proposed descriptors using random forest regression algorithms, the most important descriptors for predicting the CHF have been identified. Among the most important descriptors in the MBL, which is a novel characteristic length for the spacing between surface features.

This work has provided a framework for future ML models, which would be improved by incorporating a larger variety of surface morphology types. As more surface types are added to the model, additional descriptors may be added and tested to account for the impact new feature types on known behaviors that influence the CHF, gradually improving the scope and accuracy of the ML model.

The random forest regression method has been found to be the most effective ML method for this application, compared to neural networks and support vector regression. As the model is expanded to include more data, it may become more feasible to apply other machine learning methods, like neural networks, that work better with larger datasets.

Declaration of Competing Interest

The authors declare that they have no known competing financial interests or personal relationships that could have appeared to influence the work reported in this paper.

CRediT authorship contribution statement

Brandon Swartz: Data curation, Investigation, Methodology, Writing – original draft. **Lang Wu:** Formal analysis, Software, Methodology, Writing – original draft. **Qiang Zhou:** Methodology, Writing – review & editing. **Qing Hao:** Conceptualization, Methodology, Writing – review & editing.

Acknowledgment

Hao thanks the National Science Foundation [grant number CBET-1651840] for thermal studies. We acknowledge undergraduate researcher Jinhua Ouyang for assisting with the literature review.

Supplementary materials

Supplementary material associated with this article can be found, in the online version, at doi:10.1016/j.ijheatmasstransfer.2021.121744.

References

[1] S.S. Kutateladze, Boiling heat transfer, Int. J. Heat Mass Transf. 4 (1961) 31–45, doi:10.1016/0017-9310(61)90059-X.
[2] G. Liang, I. Mudawar, Pool boiling critical heat flux (CHF) – Part 1: review of mechanisms, models, and correlations, Int. J. Heat Mass Transf. 117 (2018) 1352–1367, doi:10.1016/j.ijheatmasstransfer.2017.09.134.
[3] G. Liang, I. Mudawar, Review of pool boiling enhancement by surface modification, Int. J. Heat Mass Transf. 128 (2019) 892–933, doi:10.1016/j.ijheatmasstransfer.2018.09.026.
[4] M.M. Rahman, E. Ölçeroğlu, M. McCarthy, Role of wickability on the critical heat flux of structured superhydrophilic surfaces, Langmuir 30 (2014) 11225–11234, doi:10.1021/la5030923.
[5] S.G. Kandlikar, A theoretical model to predict pool boiling CHF incorporating effects of contact angle and orientation, J. Heat Transf. 123 (2001) 1071–1079, doi:10.1115/1.1409265.
[6] R. Li, Z. Huang, A new CHF model for enhanced pool boiling heat transfer on surfaces with micro-scale roughness, Int. J. Heat Mass Transf. 109 (2017) 1084–1093, doi:10.1016/j.ijheatmasstransfer.2017.02.089.
[7] H.S. Ahn, C. Lee, J. Kim, M.H. Kim, The effect of capillary wicking action of micro/nano structures on pool boiling critical heat flux, Int. J. Heat Mass Transf. 55 (2012) 89–92, doi:10.1016/j.ijheatmasstransfer.2011.08.044.
[8] K.-H. Chu, R. Enright, E.N. Wang, Structured surfaces for enhanced pool boiling heat transfer, Appl. Phys. Lett. 100 (2012) 241603, doi:10.1063/1.4724190.
[9] G. Su, K. Fukuda, K. Morita, M. Pidduck, D. Jia, T. Matsumoto, R. Akasaka, Applications of artificial neural network for the prediction of flow boiling curves, J. Nucl. Sci. Technol. 39 (2002) 1190–1198, doi:10.1080/18811248.2002.9715310.
[10] X. Zhao, R.K. Salko, K. Shirvan, Machine learning-based critical heat flux predictors in subcooled and low-quality flow boiling, in: Int. Top. Meet. Adv. Therm. Hydraul., American Nuclear Society, Orlando, FL, 2018, pp. 945–948. https://www.osti.gov/biblio/1545239.
[11] A.S. Nafey, Neural network based correlation for critical heat flux in steam-water flows in pipes, Int. J. Therm. Sci. 48 (2009) 2264–2270, doi:10.1016/j.ijthermalsci.2009.04.010.
[12] N. Vaziri, A. Hojabri, A. Erfani, M. Monsefi, B. Nilforooshan, Critical heat flux prediction by using radial basis function and multilayer perceptron neural networks: a comparison study, Nucl. Eng. Des. 237 (2007) 377–385, doi:10.1016/j.nucengdes.2006.05.005.
[13] A. Mazzola, Integrating artificial neural networks and empirical correlations for the prediction of water-subcooled critical heat flux, Rev. Gén. Therm. 36 (1997) 799–806, doi:10.1016/S0035-3159(97)87750-1.
[14] W.-J. Wang, L.-X. Zhao, C.-L. Zhang, Generalized neural network correlation for flow boiling heat transfer of R22 and its alternative refrigerants inside horizontal smooth tubes, Int. J. Heat Mass Transf. 49 (2006) 2458–2465, doi:10.1016/j.ijheatmasstransfer.2005.12.021.
[15] G. Scalabrin, M. Condosta, P. Marchi, Modeling flow boiling heat transfer of pure fluids through artificial neural networks, Int. J. Therm. Sci. 45 (2006) 643–663, doi:10.1016/j.ijthermalsci.2005.09.009.
[16] Y. Qiu, D. Garg, L. Zhou, C.R. Kharangate, S.M. Kim, I. Mudawar, An artificial neural network model to predict mini/micro-channels saturated flow boiling heat transfer coefficient based on universal consolidated data, Int. J. Heat Mass Transf. 149 (2020) 119211, doi:10.1016/j.ijheatmasstransfer.2019.119211.
[17] H. Alimoradi, M. Shams, Optimization of subcooled flow boiling in a vertical pipe by using artificial neural network and multi objective genetic algorithm, Appl. Therm. Eng. 111 (2017) 1039–1051, doi:10.1016/j.applthermaleng.2016.09.114.
[18] H. Wei, G.H. Su, W.X. Tian, S.Z. Qiu, X.B. Yang, Study on the onset of nucleate boiling in narrow annular channel by genetic neural network, Int. Commun. Heat Mass Transf. 37 (2010) 596–599, doi:10.1016/j.icheatmasstransfer.2009.11.017.
[19] A.M. Bahman, S.A. Ebrahim, Prediction of the minimum film boiling temperature using artificial neural network, Int. J. Heat Mass Transf. 155 (2020) 119834, doi:10.1016/j.ijheatmasstransfer.2020.119834.
[20] M. Balcilar, A.S. Dalkilic, A. Suriyawong, T. Yiamsawas, S. Wongwises, Investigation of pool boiling of nanofluids using artificial neural networks and correlation development techniques, Int. Commun. Heat Mass Transf. 39 (2012) 424–431, doi:10.1016/j.icheatmasstransfer.2012.01.008.
[21] A. Pare, S.K. Ghosh, Surface qualitative analysis and ANN modelling for pool boiling heat transfer using Al2O3-water based nanofluids, Colloids Surfaces A 610 (2021) 125926, doi:10.1016/j.colsurfa.2020.125926.
[22] T. Sayahi, A. Tatar, M. Bahrami, A RBF model for predicting the pool boiling behavior of nanofluids over a horizontal rod heater, Int. J. Therm. Sci. 99 (2016) 180–194, doi:10.1016/j.ijthermalsci.2015.08.010.
[23] M. Hassanpour, B. Vaferi, M.E. Masoumi, Estimation of pool boiling heat transfer coefficient of alumina water-based nanofluids by various artificial intelligence (AI) approaches, Appl. Therm. Eng. 128 (2018) 1208–1222, doi:10.1016/j.applthermaleng.2017.09.066.

[24] M.K. Das, N. Kishor, Adaptive fuzzy model identification to predict the heat transfer coefficient in pool boiling of distilled water, Expert Syst. Appl. 36 (2009) 1142–1154, doi:10.1016/j.eswa.2007.10.044.
[25] M. He, Y. Lee, Application of deep belief network for critical heat flux prediction on microstructure surfaces, Nucl. Technol. 206 (2020) 358–374, doi:10.1080/00295450.2019.1626177.
[26] R. Tibshirani, Regression shrinkage and selection via the lasso, J. R. Stat. Soc. Ser. B 58 (1996) 267–288, doi:10.1111/j.2517-6161.1996.tb02080.x.
[27] F. Murtagh, Multilayer perceptrons for classification and regression, Neurocomputing 2 (1991) 183–197, doi:10.1016/0925-2312(91)90023-5.
[28] L. Breiman, Random forests, Mach. Learn. 45 (2001) 5–32, doi:10.1023/A:1010933404324.
[29] R. HECHT-NIELSEN, Theory of the backpropagation neural network, in: Neural Netw. Percept., Elsevier, 1992, pp. 65–93, doi:10.1016/B978-0-12-741252-8.50010-8.
[30] V. Nair, G.E. Hinton, Rectified linear units improve restricted Boltzmann machines, in: Proc. 27th Int. Conf. Int. Conf. Mach. Learn., 2010, pp. 807–814.
[31] D.P. Kingma, J. Ba, Adam: a method for stochastic optimization, in: 3rd Int. Conf. Learn. Represent. ICLR 2015 - Conf. Track Proc., 2014.
[32] S. Ruder, An overview of gradient descent optimization algorithms, (2016) 1–14. http://arxiv.org/abs/1609.04747.
[33] J.R. Quinlan, Induction of decision trees, Mach. Learn. 1 (1986) 81–106, doi:10.1007/BF00116251.
[34] D.A. Freedman, Bootstrapping regression models, Ann. Stat. 9 (1981) 1218–1228, doi:10.1214/aos/1176345638.
[35] B.H. Menze, B.M. Kelm, R. Masuch, U. Himmelreich, P. Bachert, W. Petrich, F.A. Hamprecht, A comparison of random forest and its Gini importance with standard chemometric methods for the feature selection and classification of spectral data, BMC Bioinform. 10 (2009) 213, doi:10.1186/1471-2105-10-213.
[36] B. Swartz, L. Wu, Q. Zhou, Q. Hao, Critical heat flux data for water and FC-72 on pin-fin surfaces, “Data in Brief” for this paper.
[37] H. Wei, H. Bao, X. Ruan, Machine learning prediction of thermal transport in porous media with physics-based descriptors, Int. J. Heat Mass Transf. 160 (2020) 120176, doi:10.1016/j.ijheatmasstransfer.2020.120176.
[38] Y. Xiao, Q. Chen, D. Ma, N. Yang, Q. Hao, Phonon transport within periodic porous structures — from classical phonon size effects to wave effects, ES Mater. Manuf. (2019) 2–18, doi:10.30919/esmm5f237.
[39] S. Mukherjee, I. Mudawar, Pumpless loop for narrow channel and microchannel boiling, J. Electron. Packag. 125 (2003) 431–441, doi:10.1115/1.1602708.
[40] K.-H. Chu, Y. Soo Joung, R. Enright, C.R. Buie, E.N. Wang, Hierarchically structured surfaces for boiling critical heat flux enhancement, Appl. Phys. Lett. 102 (2013) 151602, doi:10.1063/1.4801811.
[41] S. Kim, H.D. Kim, H.D. Kim, H.S. Ahn, H. Jo, J. Kim, M.H. Kim, Effects of nanofluid and surfaces with nano structure on the increase of CHF, Exp. Therm. Fluid Sci. 34 (2010) 487–495, doi:10.1016/j.expthermflusci.2009.05.006.
[42] H.W. Moon, Y.J. Yoon, J.H. Park, B.-S. Myung, D.E. Kim, Dynamic wetting and boiling characteristics on micro-structured and micro/nano hierarchically structured surfaces, Exp. Therm. Fluid Sci. 74 (2016) 19–26, doi:10.1016/j.expthermflusci.2015.11.019.